


Article

# A Framework for Optimal Sensor Placement to Support Structural Health Monitoring

Shen Li <sup>1</sup>, Andrea Coraddu <sup>2,\*</sup>  and Feargal Brennan <sup>1</sup>

<sup>1</sup> Department of Naval Architecture, Ocean and Marine Engineering, University of Strathclyde, Glasgow G1 1XQ, UK

<sup>2</sup> Faculty of Mechanical, Maritime and Materials Engineering, Delft University of Technology, 2600 AA Delft, The Netherlands

\* Correspondence: a.coraddu@tudelft.nl

**Abstract:** Offshore or drydock inspection performed by trained surveyors is required within the integrity management of an in-service marine structure to ensure safety and fitness for purpose. However, these physical inspection activities can lead to a considerable increase in lifecycle cost and significant downtime, and they can impose hazards for the surveyors. To this end, the use of a structural health monitoring (SHM) system could be an effective resolution. One of the key performance indicators of an SHM system is its ability to predict the structural response of unmonitored locations by using monitored data, i.e., an inverse prediction problem. This is highly relevant in practical engineering, since monitoring can only be performed at limited and discrete locations, and it is likely that structurally critical areas are inaccessible for the installation of sensors. An accurate inverse prediction can be achieved, ideally, via a dense sensor network such that more data can be provided. However, this is usually economically unfeasible due to budget limits. Hence, to improve the monitoring performance of an SHM system, an optimal sensor placement should be developed. This paper introduces a framework for optimising the sensor placement scheme to support SHM. The framework is demonstrated with an illustrative example to optimise the sensor placement of a cantilever steel plate. The inverse prediction problem is addressed by using a radial basis function approach, and the optimisation is carried out by means of an evolutionary algorithm. The results obtained from the demonstration support the proposal.

**Keywords:** structural health monitoring; optimisation; structural integrity; evolutionary algorithm; stress concentration



**Citation:** Li, S.; Coraddu, A.; Brennan, F. A Framework for Optimal Sensor Placement to Support Structural Health Monitoring. *J. Mar. Sci. Eng.* **2022**, *10*, 1819. <https://doi.org/10.3390/jmse10121819>

Academic Editors: Baran Yeter and Yordan Garbatov

Received: 27 October 2022

Accepted: 23 November 2022

Published: 25 November 2022

**Publisher's Note:** MDPI stays neutral with regard to jurisdictional claims in published maps and institutional affiliations.



**Copyright:** © 2022 by the authors. Licensee MDPI, Basel, Switzerland. This article is an open access article distributed under the terms and conditions of the Creative Commons Attribution (CC BY) license (<https://creativecommons.org/licenses/by/4.0/>).

## 1. Introduction

Ocean energy exploitation and maritime transportation are crucial elements in modern society. To ensure safe operation across the entire maritime industry, an adequate and reliable structural system that provides the required working and production spaces for crew and machinery is indispensable. Marine structures, such as offshore wind supporting foundations, ship hulls, and oil and gas production platforms, are large-scale and complex engineering systems [1]. Any failure in these systems can lead to significant loss of revenue or, potentially, a severe impact on the marine ecosystem [2]. Unfortunately, structural failures with various severities still occur from time to time in the maritime industry [3]. Catastrophic structural failures are generally the results of either progressive or shock-type deterioration. In the former, the failures are rooted in the deterioration of structural integrity over time due to the continuous exposure to a harsh marine environment, which leads to considerable fatigue crack [4–6], corrosion [7,8], dent [9], and buckling [10,11]. Concerning shock-type deterioration, it is typically due to extreme weather (e.g., storms) and/or accidental events (e.g., impact of a dropped object, slamming, etc.). These are usually accompanied by a sudden loss of the structural stiffness, potentially causing destructive failures. In this respect, a rapid identification of damage is highly relevant, e.g., eigen-perturbation

techniques [12,13]. The present study is performed in association with progressive deterioration, and in this context, a dedicated structural integrity management scheme is required [14] to limit the probability of failure below an acceptable level throughout the entire life span. A structural integrity management program typically consists of data, an evaluation, a strategy, and a program [15]. Traditionally, structural condition data are collected through physical inspection, where qualified surveyors are periodically sent offshore, or when the structure is in drydock. Most inspections rely principally on visual examination, which is supported by local thickness measurements and non-destructive evaluation (NDE) techniques in the areas of interest. However, a conventional surveyor inspection may be subjected to accessibility and the availability issues. The accessibility of structurally critical details may be highly limited if they are in hard-to-reach areas. In terms of availability, some structural components may not be available for inspection due to an on-going production activity. Furthermore, unexpected adverse weather (e.g., storms) could cause delays in inspections. All of these issues could potentially cause some concerning structural damages to be overlooked. In addition, physical inspection requires the surveyors to work in a hazardous environment, imposing health and safety risks for the surveyors. Another concern is related to human errors, since this activity depends on the inspector's perception and experience to a fairly large extent. Even though the foregoing matters have been adequately addressed, physical inspection, particularly in drydock, may result in significant downtime of the assets [16].

To this end, there has been a broad spectrum of efforts to install various sensing units on board in order to monitor the structural condition remotely and continuously so that the interference in the production activities can be minimised [17]. The monitored data (e.g., stress/strain response) serve as inputs for dedicated condition assessment modules, such as cumulative fatigue and crack growth assessment modules [18], in order to assess the health of the structures. This can then assist the management of lifetime structural integrity and possibly demonstrate the case for life extension, known as in structural health monitoring [19].

Many approaches are available within SHM, e.g., vibration-based monitoring, strain monitoring, acoustic emission, etc. [20]. One of the advantages of a key performance indicator of SHM, strain (or displacement) monitoring, is its ability to predict the structural response of unmonitored locations by using monitored data, i.e., an inverse prediction problem [21–23]. This is highly relevant in practical engineering, since monitoring can only be performed at limited and discrete locations, and it is likely that unmonitored locations are structurally critical, but unfeasible for installing sensors. This inverse prediction capability is also pertinent in the development of digital-twin-based monitoring. As demonstrated by [24], digital-twin-based monitoring can be implemented with the aid of a selection of structural response measurements and an inverse problem solver so that holistic structural monitoring can be achieved. In either case, the accuracy of the inverse prediction is dependent on the number of sensors [25]. It is desirable to install as many sensors as practically possible so that more data can be provided to the inverse problem solver, as shown, for instance, in [26]. However, this is often constrained by the available budget. In the meantime, the amount of data is also a barrier that affects the practicality of implementing an SHM system (e.g., data storage and data communication from offshore to onshore). Thus, the locations of the employed sensors should be carefully determined.

In light of this, an optimisation framework is formulated in this paper with the objective of optimising the sensor installation locations whilst ensuring an acceptable accuracy of the inverse prediction problem. The proposed framework consists of: (i) a forward problem to provide input data, (ii) an inverse problem to address the inverse prediction, and (iii) optimisation to derive the optimal placement solution. The framework is demonstrated with an illustrative example in which the input data are provided by experimental measurements, and the inverse problem is addressed with a radial basis function (RBF) [27]. This is combined with the genetic algorithm [28] to develop the optimal sensor placement of a strain gauge rosette array for a cantilever steel plate.

The paper is organised as follows. Section 2 provides a review of related academic studies and industrial standards, followed by a definition of the generalised framework in Section 3. Thereafter, an illustrative example is presented in Section 4 to demonstrate the proposed framework and to discuss the benefits of sensor placement optimisation. Finally, the main conclusions and recommendations for future research are discussed in Section 5.

## 2. Literature Review

A literature survey on optimal sensor placement was conducted by [29]. It was indicated that whilst SHM has seen a wide range of applications in various engineering fields, research and developments related to sensor placement optimisation are limited. Optimisation of sensor placement for a cross-stiffened panel subjected to lateral pressure was presented by [30]. The inverse finite element method was combined with an optimisation framework that leveraged a genetic-algorithm-based solver. A 70% reduction of the sensor number was achieved, while the loss in monitoring accuracy was merely 0.6%. The authors of [31] applied sequential space filling, the genetic algorithm, and the simulated annealing algorithm to optimise the sensor placement of a steel-frame structure. It was shown that the simulated annealing algorithm was the most effective for the problem of interest. A Bayesian optimisation framework for deriving optimal sensor network design for SHM with the Bayes risk as the objective function was proposed by [32]. This was motivated by the fact that the prediction of the structural state is associated with cost/risk due to various known or unknown uncertainties. Using the Bayes risk as the objective function can lead to the least expected loss/risk as a consequence of making decisions on the structural state. The optimisation of a multi-axial-displacement sensor placement was investigated by [33]. A tri-axial modal assurance criterion was developed by taking three translational degrees of freedom into account as a single unit in a Fisher information matrix. The proposed criterion was combined with a distributed wolf algorithm to determine the optimal sensor placement of a benchmark frame structure. The artificial bee colony algorithm combined with the modal assurance criterion was employed by the authors of [34] to develop the optimal sensor placements of a 27-bar truss bridge, a 21-storey building, and a high tower. Mallardo et al. [35] studied the sensors' optimal locations for identifying impacts on composite structures. In this study, piezoelectric sensors were applied to estimate the location of the impact. In order to reduce the computational effort, the authors adopted an artificial neural network (ANN) to evaluate the objective function.

Standards and recommended practices are issued by various maritime authorities with regard to the specification of monitoring systems, e.g., DNV [36], ABS [37], ClassNK [38], and GL [39]. The specifications include the sensor type, sampling rate, acceptable uncertainty tolerance, and installation methods. Except for the minimum number of required sensors, it appears that no recommendations have been provided in connection with the optimisation of sensor placement.

## 3. Sensor Optimisation Framework

A sensor optimisation framework for optimising sensor placement is defined in this paper. The principle of the proposed framework is elucidated via the flowchart shown in Figure 1. Three key elements are considered: (i) a forward problem, (ii) an inverse problem, and (iii) optimisation. It is generally applicable to the determination of the optimal sensor placement for structures of which the structural states are known or can be simulated.

The forward problem refers to the prediction of the structural response to external environmental actions, such as wind, waves, and currents. It is relevant in the present context as a means of providing input (training and testing data) for the inverse problem and optimisation. The responses can be collected with physical measurements or through an equivalent simulation in which virtual measurements can be taken.

As briefly mentioned in the previous section, the inverse problem addresses the prediction of a selected number of training data, e.g., the prediction of the unmonitored response by using a monitored response with reference to SHM applications. A data-driven

or physics-based algorithm can be employed [40]. The accuracy of the inverse prediction is assessed in comparison with the testing data (i.e., the predicted testing data versus the actual testing data), where the inverse problem solver provides the predicted testing data.

An appropriate optimisation algorithm is applied in order to derive an optimal set of training data, i.e., the optimal sensor placement, which minimises the error of the inverse prediction.

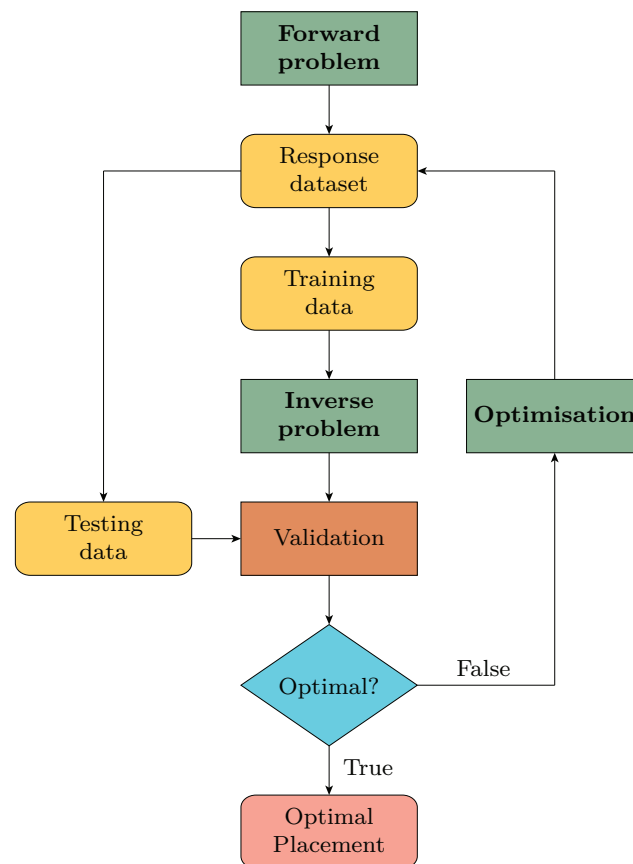


**Figure 1.** Proposed generalised methodology for optimising the sensor placement.

#### 4. Illustrative Example

To demonstrate, in a tractable manner, the fundamental concept of the methodology described in Section 3, an elementary optimisation problem is considered, and it aims to seek the best placement of a strain gauge array for measuring the stress field near a stress concentration area. This illustrative example is a practical engineering problem that is relevant for the structural health monitoring of local structural details with an abrupt change in the geometry and, consequently, stress concentrations, e.g., in plate-stiffener intersections or tubular joints of offshore structures. Hence, the obtained results would have a direct impact in terms of guiding the design and specifications of a monitoring system for local hotspots.

##### 4.1. Problem Statement

Structural details with an abrupt change in their geometry are usually associated with a considerable stress gradient [1]. Therefore, using a monitoring array formed by multiple strain gauges would be more suitable than using a single strain gauge [41]. Moreover, the strain gauge array benefits the overall monitoring system by adding redundancy, so the robustness of the system against sensor malfunction can be enhanced [42].

A structural test was performed on a 1 m × 1 m perforated steel plate instrumented with a fibre Bragg grating (FBG) strain gauge array (Figure 2). The FBG strain gauge array has several benefits. It is immune to electromagnetic interference and intrinsically passive,

i.e., no electrical power is necessary; therefore, it can be positioned in areas with a high voltage and potentially explosive atmosphere. Moreover, it has multiplexing capabilities. More than 20 FBGs can be located in a single fibre.

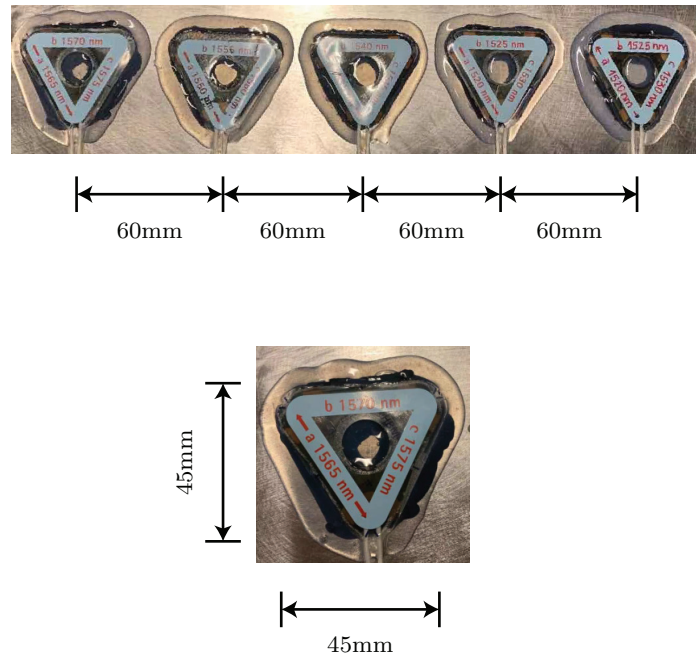


**Figure 2.** A strain gauge array formed of five fibre Bragg grating rosettes.

As schematically illustrated in Figure 3, the test specimen (perforated plate) is fixed to the horizontal rigid support via three angle brackets. The opposite end is subjected to a pressure load imparted by the incoming waves. This configuration effectively results in a cantilever plate condition. A 0.2 m × 0.2 m hole is introduced at the centre of the plate to simulate the stress concentration. A finite element analysis indicates that a hotspot occurs at the upper corner of the square hole, and thus, the strain gauge array is installed in this area. The strain gauge array adopted in the present test is formed of five rosettes, as reported in Figure 2.

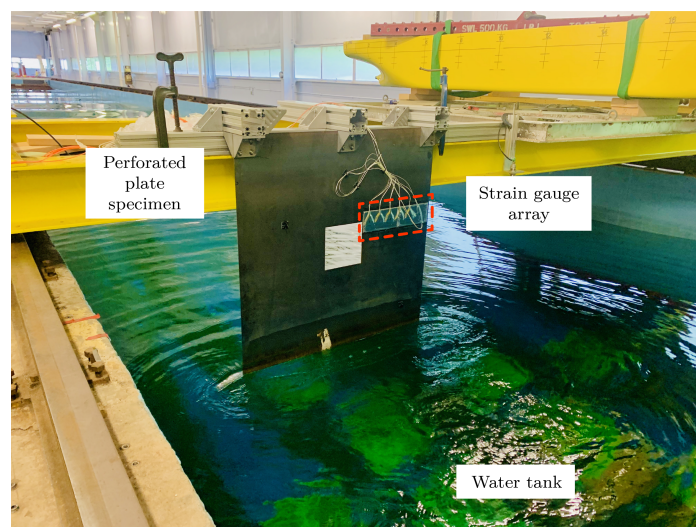


**Figure 3.** Structural test of perforated plate instrumented with FBG.

Each strain gauge rosette is of a delta shape, with three individual sensors oriented at 0°, 60°, and 120°. The footprint of an individual rosette is approximately 45 mm × 45 mm.

The centre-to-centre distance between the adjacent rosettes is 60 mm, and the distance between the first rosette and the square hole corner is 35 mm. Under the lateral pressure load induced by an incoming wave with a frequency of 0.8 Hz and amplitude of 75 mm, the distribution of the maximum von Mises stress is shown in Figure 4.

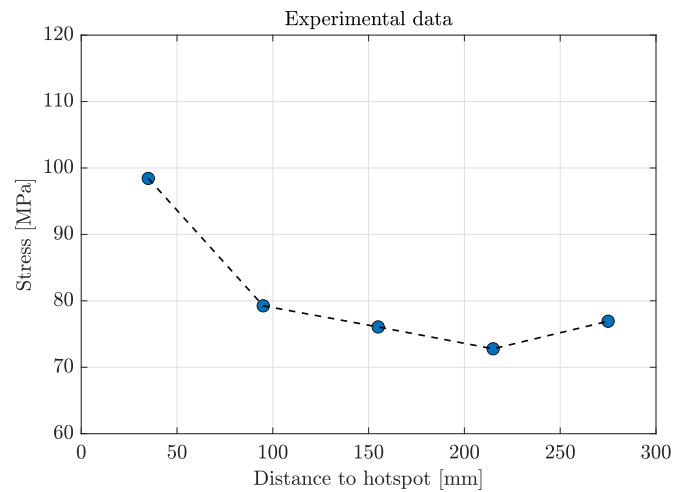


Figure 4. Test data.

The primary aim of the present study is to optimise the proposed strain gauge array by reducing the number of rosettes from five to three and determining the optimal installation locations that minimise the prediction error of the inverse prediction model. In this study, the prediction error is assessed with a comparison between the predicted stresses and the experimentally measured stresses for the five locations in which physical measurements are conducted. This can be easily remapped into a classic single-objective optimisation problem. Thus, three variables are involved in the optimisation, namely, the coordinate of rosette No. 1 ( $x_a$ ), the coordinate of rosette No. 2 ( $x_b$ ), and the coordinate of rosette No.3 ( $x_c$ ), as reported in Table 1. As a comparison, the optimal sensor placement of a four-rosette strain gauge array is also considered (i.e., an additional variable: coordinate of rosette No. 4— $x_d$ ). The optimisation problem is similar, and thus, for the sake of brevity, its formulation is not elaborated here. Note that the coordinate refers to the centroid of each rosette.

Table 1. Summary of variables to be optimised.

Variable	Symbol	Unit
Centroid of rosette $a$	$x_a$	mm
Centroid of rosette $b$	$x_b$	mm
Centroid of rosette $c$	$x_c$	mm

Within the optimisation, if candidate solutions (i.e., the locations of the rosettes) are determined, the responses of these locations will be evaluated through the interpolation (based on the test data) of the two adjacent measurement locations. An inverse prediction will then be performed to provide response predictions for all five actual measurement locations ( $\tilde{\sigma}$ ) where test data are available ( $\sigma$ ). In the present paper, an RBF-based approach is employed for the inverse prediction. For each prediction, its difference from the test data gives a prediction error ( $e$ ). The five prediction errors give an error vector ( $\mathbf{e}$ ). The sum of the second norm and the infinite norm of the error vector provides a measure of the prediction performance [43] and is the objective of the present optimisation, i.e., minimisation. The second norm emphasises the overall performance of the prediction, and the infinite norm targets the maximum error to ensure that no significant outlier would exist. The relative importance of the second norm and infinite norm can also be formulated in the objective function by using a weighting factor. An alternative definition of the objective function

is possible; e.g., the reader is referred to [44], where the use of the  $f$ -divergence as the objective function was investigated for optimal sensor placement.

Two groups of constraints are considered in the optimisation. Firstly, each rosette must be located within the current footprint of the entire array. To this end, the optimal value of each variable can only be searched within a constrained interval. The lower and upper bounds of each variable are summarised in Table 2.

**Table 2.** Summary of the lower and upper bounds of the variables.

Variable	Lower Bound		Upper Bound		Unit
	Symbol	Value	Symbol	Value	
Centroid of rosette $a$	$x_a^l$	0	$x_a^u$	240	mm
Centroid of rosette $b$	$x_b^l$	0	$x_b^u$	240	mm
Centroid of rosette $c$	$x_c^l$	0	$x_c^u$	240	mm

Secondly, no overlapping of rosettes is allowed. Since each rosette has a physical size (45 mm × 45 mm in the present case), the centroid-to-centroid distance should be specified to avoid any overlapping. In the installation of the present test, the centroid-to-centroid distance was determined to be 60 mm. Considering the physical size of the deployed rosettes and the extra space for the waterproofing treatment, this appeared to be smallest practical distance after consultation with an installation technician.

4.2. Formulation and Solution Scheme for Optimisation

In accordance with the descriptive problem statement given in the previous section, the scope of the present optimisation is to minimise the weighted sum of the second norm ( $\|\mathbf{e}\|_{\ell^2}$ ) and the infinite norm ( $\|\mathbf{e}\|_{\ell^\infty}$ ) of the error vector, i.e.,  $\mathbf{e} = \{e_1, e_2, e_3, e_4, e_5\}$ . The weighting factor is denoted as  $\alpha$ . The error vector consists of the prediction errors of five tested locations (see Figure 2). Each error entry is evaluated as the difference between the predicted response ( $\tilde{\sigma}_i$ ) and the experimentally measured response ( $\sigma_i$ ), i.e.,  $e_i = \tilde{\sigma}_i - \sigma_i$ , where  $i = 1, 2, 3, 4, 5$ .

More formally, a mathematical formulation of the optimisation problem (three-rosette array) can be written as follows:

$$\begin{aligned}
 & \min_{x_a, x_b, x_c \in \mathbb{R}} \alpha \|\mathbf{e}\|_{\ell^2} + (1 - \alpha) \|\mathbf{e}\|_{\ell^\infty} & (1) \\
 & \text{subject to} \quad \begin{cases} x_a^l \leq x_a \leq x_a^u \\ x_b^l \leq x_b \leq x_b^u \\ x_c^l \leq x_c \leq x_c^u \\ |x_a - x_b| \geq \Delta x_{min} \\ |x_a - x_c| \geq \Delta x_{min} \\ |x_b - x_c| \geq \Delta x_{min} \end{cases}
 \end{aligned}$$

The lower and upper bounds of each variable are provided in Table 2. The predicted response is derived by solving the inverse problem by using an RBF approach with the responses  $\sigma_a, \sigma_b,$  and  $\sigma_c$  at three candidate rosette locations  $x_a, x_b,$  and  $x_c$  as the input:

$$\tilde{\sigma}_i = f_{RBF}(x_a, x_b, x_c, x_i) \tag{2}$$

The RBF is able to perform interpolation based on an irregular grid; therefore, it is suitable for the problem of interest in this paper, since the rosettes are likely to be distributed in an irregular manner (i.e., with a varying spacing). Meanwhile, the measurements are retained in the developed predictive algorithm, i.e., the predictions for the monitored

locations will be the same as the actual measurements. In fact, the application of other data-driven algorithms is possible, and according to the No Free Lunch Theorem for Machine Learning, which states that the performance of all algorithms is equally good, several classes of algorithms should be tested [45]. An RBF is centrally symmetric with respect to a specific point. In the present context, these specific points refer to  $x_a$ ,  $x_b$ , and  $x_c$ . The RBF value at any other location can be represented as follows:

$$\varphi(x) = \varphi(\|x - x_0\|) \tag{3}$$

where  $\|x - x_0\|$  effectively refers to the distance between the point of interest  $x$  and the fixed point  $x_0$ . As reported by Equation (4), a Gaussian function is a typical RBF.

$$\varphi(x) = \exp\left(-\frac{\|x - x_0\|^2}{2\sigma^2}\right) \tag{4}$$

The parameter  $\sigma$  controls the smoothness of the interpolated function. It can be estimated as the average distance between any two points in an irregular grid. The RBF-based interpolated function can then be formulated as the weighted sum of a series of RBFs, each of which centres around one of the training data points:

$$f_{RBF}(x) = \sum_{j=1}^m w_j \varphi(\|x - x_j\|) \tag{5}$$

where  $x_j$  is the spatial coordinate of the data point and  $m$  is the number of data points. The weight coefficients  $w_j$  are determined by imposing the requirement that the interpolated value at the training data point is identical to the corresponding actual value, and thus,

$$f_{RBF}(x_j) = f_{actual}(x_j) \tag{6}$$

In the present context,  $m = 3$  because three rosettes (at  $x_a$ ,  $x_b$ , and  $x_c$ , respectively) are considered, and accordingly, the actual values at these locations are  $\sigma_a$ ,  $\sigma_b$ , and  $\sigma_c$ . Thus, by applying Equations (5) and (6) to the present problem of interest, a system of linear equations with three unknowns can be developed:

$$\begin{bmatrix} \varphi(\|x_a - x_a\|) & \varphi(\|x_a - x_b\|) & \varphi(\|x_a - x_c\|) \\ \varphi(\|x_b - x_a\|) & \varphi(\|x_b - x_b\|) & \varphi(\|x_b - x_c\|) \\ \varphi(\|x_c - x_a\|) & \varphi(\|x_c - x_b\|) & \varphi(\|x_c - x_c\|) \end{bmatrix} \begin{Bmatrix} w_a \\ w_b \\ w_c \end{Bmatrix} = \begin{Bmatrix} \sigma_a \\ \sigma_b \\ \sigma_c \end{Bmatrix} \tag{7}$$

Once Equation (7) is solved and the weight coefficients are derived, the estimated response at the testing location (i.e.,  $\sigma_i$  with  $i = 1, 2, 3, 4, 5$ ) can be obtained, as shown by Equation (2). The experimentally measured response is denoted as

$$\sigma_i = f_{Exp}(x_i) \tag{8}$$

The entry of the error vector (i.e.,  $\mathbf{e}$  in Equation (1)) can then be expressed as

$$e_i = \check{\sigma}_i - \sigma_i = f_{RBF}(x_a, x_b, x_c, x_i) - f_{Exp}(x_i) \tag{9}$$

With respect to the optimisation solver, a genetic algorithm [28] implemented in the Matlab environment is adopted. This is a well-suited approach for nonlinear and non-convex objectives, as given by Equation (1). In principal, the algorithm involves the following evolutionary process: elitism, selection, crossover, and mutation. A population of possible solutions to the problem of interest is randomly initialised to form the first generation. The number of possible solutions defines the size of the generated population. An individual solution within the population is executed by the inverse problem solver to evaluate the corresponding objective function. When this evaluation is completed for all individuals, the objective functions are ranked to identify the best fit. Note that the best-fit



solution is propagated to the next generation because of elitism. Once the evaluation and ranking of objective functions are completed, a tournament selection is applied to select the “parents”. The tournament operation selects  $k$  individuals from the population with  $k > 2$  as “parents”. The repeating of the tournament selection is terminated when a desired number of “parents” are available. The paired parents will carry out a crossover operation, which simulates genetic recombination, as in human reproduction. Following the crossover operation, each offspring is submitted to a mutation operation, which is a small random tweak in the chromosome to obtain a new solution. This is used to maintain and introduce diversity in the genetic population. The specifications of the applied genetic algorithm are summarised in Table 3.

**Table 3.** Summary of the settings of the genetic algorithm’s specifications.

Specification	Setting
Population	1000
Elite count	50

4.3. Results

The optimal sensor placements of a strain gauge array with three and four rosettes are illustrated in Figure 5.

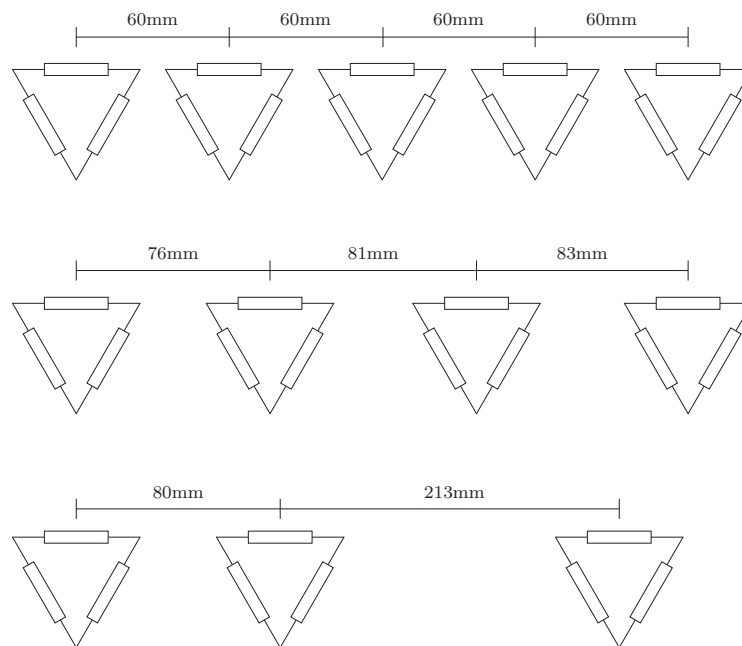


**Figure 5.** Comparison between the initial five-rosette strain gauge array and the optimised four-rosette and three-rosette arrays.

These results were obtained by assuming an equal importance between the second norm and the infinite norm of the error vector, i.e.,  $\alpha = 0.5$ . In comparison with the initial placement, the optimised array shows a varying spacing, in which a smaller spacing is used if the rosette is placed closer to the hotspot. This reflects the underlying structural response well, since a higher stress gradient occurs in proximity to the hotspot, whereas the stress response would converge as it becomes further away from the stress concentration area. As illustrated in Figures 6 and 7, the interpolations based on the optimised array with three or four rosettes are comparable with the actual measurements.

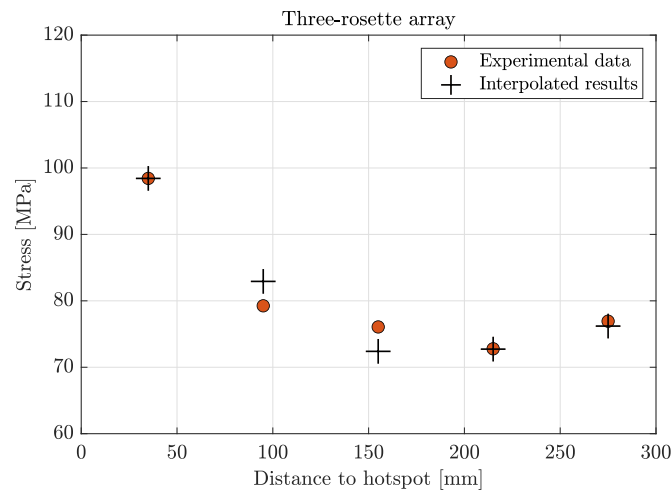


**Figure 6.** Comparison between the experimental measurements and interpolated results based on an optimised rosette placement.

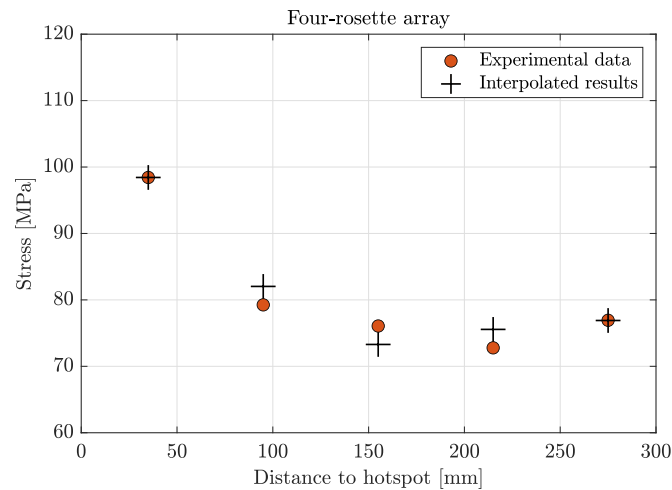


**Figure 7.** Comparison between the experimental measurements and interpolated results based on an optimised rosette placement.

To investigate the effect of the weighting factor  $\alpha$ , two additional cases with  $\alpha = 0.3$  and  $\alpha = 0.7$  are considered. The first case emphasises the importance of the infinite norm, and the second case emphasises the second norm. The results are compared in Table 4. It can be seen that the weighting factor has a negligible influence on this one-dimensional problem, where the inverse prediction shows a high accuracy and, thus, the difference between the second norm and the infinite norm is marginal. However, a greater influence is expected when the problem is extended to two or three dimensions. This will become the subject of future studies.

The results reported above demonstrate the promising application of an optimisation algorithm for the development of optimal sensor placements, such that comparable performance can be achieved with respect to a dense sensor network. Although the present illustrative example is a one-dimensional problem in which the location of each sensor is described only by a coordinate in one dimension, it demonstrates, in a tractable manner, how an optimisation of sensor placement can be performed and its value in practical engineering. Additionally, this capability is of great significance in the design and offshore application of FBG strain gauge arrays comprising multiple sensors. Thanks to the multiplexing feature, all sensors in an FBG array can share the same fibre. The signals can then be streamed to the interrogator via one channel. However, there is a limit with regard to the number of signals (i.e., the number of sensors) with which each channel can cope. For instance,

the initial five-rosette array can be problematic, since the signals ( $3 \times 5 = 15$  signals in total) may need to be clustered to the interrogator through more than one channel. This somewhat counteracts the benefit of multiplexing and has an impact on the number of monitoring locations that a single interrogator can manage. In addition, the extra wiring and relevant protection measures give rise to an increase in the fitting cost and difficulty. The increase in cost can be considerable for a large-scale offshore structure. In terms of limitations, the measurement noise, uncertainty, and bias are not taken into account, but this is recommended for future studies.

**Table 4.** Optimal sensor placement: three-rosette array.

Weighting Factor	Rosette Position	Value	Unit
$\alpha = 0.5$	$x_a$	0	mm
	$x_b$	80	mm
	$x_c$	213	mm
$\alpha = 0.3$	$x_a$	0	mm
	$x_b$	80	mm
	$x_c$	214	mm
$\alpha = 0.7$	$x_a$	0	mm
	$x_b$	80	mm
	$x_c$	213	mm

### 5. Conclusions

A dedicated structural integrity management program is a crucial element in ensuring the safety of offshore structures that operate in a hostile marine environment. One of the fundamental aspects of structural integrity management is the collection of structural condition data, which enable the assessment of the health of in-service structures in order to determine their fitness for purpose and whether intervention is needed. The traditional surveyor inspection approach is challenged by a number of technical obstacles: inspection accessibility and availability, health and safety of surveyors, human error, and infrastructure downtime. To this end, a structural health monitoring (SHM) system can be employed. By installing sensors on board, an SHM system enables remote and continuous monitoring of the integrity of an in-service structure. Apart from eliminating the drawbacks related to surveyor inspections, SHM also has the potential to be incorporated into a digital-twin-based monitoring framework. One of the key capabilities of the SHM system is the prediction of the responses of unmonitored locations by using monitored data. An ideal scenario would be to collect as much data as practically possible so that a good amount of data can be provided to address the inverse problem. However, a limited budget appears to be the constraint of SHM system design. Thus, to support SHM systems, an optimisation of the sensor placement is required to provide optimal performance.

In light of this, a sensor placement optimisation framework was developed in this paper. A radial basis function was employed to address the inverse prediction, while the genetic algorithm was adopted for optimisation. An illustrative example of the design of an FBG strain gauge array was provided to demonstrate the methodology. Two scenarios were considered, where the number of rosettes was reduced from five to three or four. The results showed that the reduced set of rosettes with the optimised placement was comparable with the initial dense network. The proposed framework can contribute to the initial development of sensor packages for a monitoring system (i.e., the specification of sensor locations and numbers). Additionally, it has the potential to be integrated into a monitoring system to dynamically inform users about the optimal set of sensor data. In other words, sensors that provide a less critical data stream for a specific scenario can be temporarily turned off. Consequently, the amount of data can be dramatically reduced, and this will be hugely beneficial in terms of data storage and data communication from offshore to onshore.

The present preliminary study opens a number of opportunities for future research. The illustrative example reported in this paper is a one-dimensional problem with respect to the variable, i.e., sensor location. Future research can be carried out to extend the dimensionality of the variables, such that the effectiveness of the proposed optimisation can be further evaluated. To improve the effectiveness of the proposed optimisation for a multi-dimensional problem, advanced algorithms for addressing inverse prediction are needed. For instance, modal decomposition and expansion theory appears to be a capable method for SHM that has been a subject of great interest in recent years. However, the combination of this theory and an optimisation algorithm for the development of optimal sensor placement has not yet been detailed; hence, this is recommended as future research. Moreover, the consideration of missing data streams may deserve future study. A plausible approach is that of refining the objective function by taking account of the prediction accuracy based on a partial data stream. An appropriate weighting factor may be required to reflect the differences in the likelihood of each malfunctioning event. Future work can be performed to investigate the feasibility of this idea. Further, measurement noise or bias was not accounted for in the illustrative example, and it should be addressed in future research.

**Author Contributions:** S.L.: Conceptualisation, methodology, software, formal analysis, validation, writing—original draft preparation, and writing—review and editing; A.C.: Conceptualisation, methodology, software, formal analysis, validation, writing—original draft preparation, writing—review and editing, project administration, and funding acquisition; F.B.: Writing—review and editing, project administration, and funding acquisition. All authors have read and agreed to the published version of the manuscript.

**Funding:** This research received no external funding.

**Conflicts of Interest:** The authors declare no conflict of interest.

## Abbreviations

The following abbreviations are used in this manuscript:

FBG	Fibre Bragg grating
SHM	Structural health monitoring
RBF	Radial basis function
DT	Digital twin
GA	Genetic algorithm

## References

1. Lotsberg, I. *Fatigue Design of Marine Structures*; Cambridge University Press: Cambridge, UK, 2016.
2. Yao, T.; Fujikubo, M. *Buckling and Ultimate Strength of Ship and Ship-like Floating Structures*; Butterworth-Heinemann: Oxford, UK, 2016.
3. Paik, J.K. *Advanced Structural Safety Studies: With Extreme Conditions and Accidents*; Springer: Berlin/Heidelberg, Germany, 2020.
4. Wong, E.W.C.; Kim, D.K. A simplified method to predict fatigue damage of TTR subjected to short-term VIV using artificial neural network. *Adv. Eng. Softw.* **2018**, *126*, 100–109. [[CrossRef](#)]
5. Yeter, B.; Garbatov, Y.; Guedes Soares, C. Fatigue damage assessment of fixed offshore wind turbine tripod support structures. *Eng. Struct.* **2015**, *101*, 518–528. [[CrossRef](#)]
6. Yeter, B.; Garbatov, Y.; Guedes Soares, C. Evaluation of fatigue damage model predictions for fixed offshore wind turbine support structures. *Int. J. Fatigue* **2016**, *87*, 71–80. [[CrossRef](#)]
7. Paik, J.K.; Kim, D.K. Advanced method for the development of an empirical model to predict time-dependent corrosion wastage. *Corros. Sci.* **2012**, *63*, 51–58. [[CrossRef](#)]
8. Mohd, M.H.; Kim, D.K.; Kim, D.W.; Paik, J.K. A time-variant corrosion wastage model for subsea gas pipelines. *Ships Offshore Struct.* **2014**, *9*, 161–176. [[CrossRef](#)]
9. Witkowska, M.; Guedes Soares, C. Ultimate strength of locally damaged panels. *Thin-Walled Struct.* **2015**, *97*, 225–240. [[CrossRef](#)]
10. Saad-Eldeen, S.; Garbatov, Y.; Guedes Soares, C. Buckling collapse tests of deteriorated steel plates with multiple circular openings. *Ocean Eng.* **2019**, *172*, 523–530. [[CrossRef](#)]
11. Li, S.; Hu, Z.Q.; Benson, S. An analytical method to predict the buckling and collapse behaviour of plates and stiffened panels under cyclic loading. *Eng. Struct.* **2019**, *199*, 109627. [[CrossRef](#)]

12. Bhowmik, B.; Tapas, T.; Budhaditya, H.; Vikram, P. First-Order Eigen-Perturbation Techniques for Real-Time Damage Detection of Vibrating Systems: Theory and Applications. *Appl. Mech. Rev.* **2019**, *71*, 060801. [[CrossRef](#)]
13. Bhowmik, B.; Krishnan, M.; Hazra, B.; Pakrashi, V. Real-time unified single- and multi-channel structural damage detection using recursive singular spectrum analysis. *Struct. Health Monit.* **2019**, *18*, 563–589. [[CrossRef](#)]
14. Yeter, B.; Garbatov, Y.; Guedes Soares, C. Risk-based maintenance planning of offshore wind turbine farms. *Reliab. Eng. Syst. Saf.* **2020**, *202*, 107062. [[CrossRef](#)]
15. O'Connor, P.E.; Bucknell, J.R.; DeFranco, S.J.; Westlake, H.S.; Puskar, F.J. Structural integrity management (SIM) of offshore facilities. In *Offshore Technology Conference*; OnePetro: Richardson, TX, USA, 2005.
16. Kolios, A.; Cevasco, D.; Wendelborn, C.S.; Baonza, C.Y. Final Report on Best Practice Guidelines for Future WF Structural Condition Monitoring Using Low-Cost Monitoring. 2022. Available online: <https://www.romeoproject.eu/wp-content/uploads/2022/06/D4.6-Final-report-on-best-practise-guidelines.pdf> (accessed on 26 October 2022).
17. Sielski, R.A. Ship structural health monitoring research at the Office of Naval Research. *JOM* **2012**, *64*, 823–827. [[CrossRef](#)]
18. Phelps, B.; Morris, B. Review of Hull Structural Monitoring Systems for Navy Ships. 2013. Available online: <https://apps.dtic.mil/sti/citations/ADA588962> (accessed on 26 October 2022).
19. Kaminski, M.L. Sensing and understanding fatigue lifetime of new and converted FPSOs. In *Offshore Technology Conference*; OnePetro: Richardson, TX, USA, 2007.
20. May, P.; Mendy, G.; Tallett, P. Structural integrity monitoring: Review and appraisal of current technologies for offshore applications. In Proceedings of the ASME 2008 27th International Conference on Offshore Mechanics and Arctic Engineering, Estoril, Portugal, 15–20 June 2009.
21. Augustyn, D.; Smolka, U.; Tygesen, U.T.; Ulriksen, M.D.; Sørensen, J.D. Data-driven model updating of an offshore wind jacket substructure. *Appl. Ocean Res.* **2020**, *104*, 102366. [[CrossRef](#)]
22. Augustyn, D.; Smolka, U.; Tygesen, U.T.; Ulriksen, M.D.; Sørensen, J.D. Feasibility of modal expansion for virtual sensing in offshore wind jacket substructures. *Mar. Struct.* **2021**, *79*, 103019. [[CrossRef](#)]
23. Henkel, M.; Häfele, J.; Weijtjens, W.; Devriendt, C.; Gebhardt, C.G.; Rolfes, R. Strain estimation for offshore wind turbines with jacket substructures using dual-band modal expansion. *Mar. Struct.* **2020**, *71*, 102731. [[CrossRef](#)]
24. Sireta, F.X.; Storhaug, G. A modal approach for holistic hull structure monitoring from strain gauges measurements and structural analysis. In Proceedings of the Offshore Technology Conference, Houston, TX, USA, 5 May 2022.
25. Papadimitriou, C. Pareto optimal sensor locations for structural identification. *Comput. Methods Appl. Mech. Eng.* **2005**, *194*, 1655–1673. [[CrossRef](#)]
26. Huang, Y.; Ludwig, S.A.; Deng, F.D. Sensor optimization using a genetic algorithm for structural health monitoring in harsh environments. *J. Civ. Struct. Health Monit.* **2016**, *6*, 509–519. [[CrossRef](#)]
27. Press, W.H.; Teukolsky, S.A.; Vetterling, W.T.; Flannery, B.P. *Numerical Recipes: The Art of Scientific Computing*; Cambridge University Press: Cambridge, UK, 2007.
28. Schmitt, L.M. Theory of genetic algorithms. *Theor. Comput. Sci.* **2001**, *259*, 1–61. [[CrossRef](#)]
29. Ostachowicz, W.; Soman, R.; Malinowski, P. Optimization of sensor placement for structural health monitoring: A review. *Struct. Health Monit.* **2019**, *18*, 963–988. [[CrossRef](#)]
30. Ghasemzadeh, M.; Kefal, A. Optimization of sensor placement for stiffened marine panels using coupled genetic algorithm and inverse finite element method. In Proceedings of the 34th Asian-Pacific Technical Exchange and Advisory Meeting on Marine Structures TEAM 2020/21, Istanbul, Turkey, 6–8 December 2021.
31. Mistarihi, M.Z.; Kong, Z.Y. Sensor Placement Optimization and Modeling for Structural Health Monitoring. *Int. J. Ind. Electron. Electr. Eng.* **2019**, *7*, 2349–204X.
32. Yang, Y.C.; Chadha, M.; Hu, Z.; Todd, M.D. An optimal sensor placement design framework for structural health monitoring using Bayes risk. *Mech. Syst. Signal Process.* **2022**, *168*, 108618. [[CrossRef](#)]
33. Yi, T.H.; Li, H.N.; Wang, C.W. Multiaxial sensor placement optimization in structural health monitoring using distributed wolf algorithm. *Struct. Control Health Monit.* **2016**, *23*, 719–734. [[CrossRef](#)]
34. Sun, H.; Büyüköztürk, O. Optimal sensor placement in structural health monitoring using discrete optimization. *Smart Mater. Struct.* **2015**, *24*, 125034. [[CrossRef](#)]
35. Mallardo, V.; Zahra, S.K.; Aliabadi, F.M.H. A Bayesian approach for sensor optimisation in impact identification. *Materials* **2016**, *9*, 946. [[CrossRef](#)] [[PubMed](#)]
36. DNV. Rules for classification: Ships—DNV-RU-SHIP Part 6 Chapter 9, Survey Arrangement. 2021. Available online: <https://www.dnv.com/news/rules-for-classification-of-ships-july-2021-edition-203529> (accessed on 26 October 2022).
37. ABS. Guide for Hull Condition Monitoring Systems. 2020. Available online: <https://www.amazon.com/Guide-Hull-Condition-Monitoring-Systems/dp/B0025LVCKY> (accessed on 27 October 2022).
38. NK. Rules for Classification and Construction: Ship Technology. 2021. Available online: <https://docslib.org/doc/1179626/rules-for-classification-and-construction-i-ship-technology> (accessed on 27 October 2022).
39. GL. Rules for Classification and Construction: Ship Technology. 2013. Available online: [https://www.academia.edu/en/10856770/Rules\\_for\\_Classification\\_and\\_Construction\\_I\\_Ship\\_Technology\\_1\\_Seagoing\\_Ships\\_5\\_Structural\\_Rules\\_for\\_Container\\_Ships\\_Edition\\_2013](https://www.academia.edu/en/10856770/Rules_for_Classification_and_Construction_I_Ship_Technology_1_Seagoing_Ships_5_Structural_Rules_for_Container_Ships_Edition_2013) (accessed on 27 October 2022).

40. Li, S.; Coraddu, A.; Oneto, L. Computationally aware estimation of ultimate strength reduction of stiffened panels caused by welding residual stress: From finite element to data-driven methods. *Eng. Struct.* **2022**, *264*, 114423. [[CrossRef](#)]
41. Cusano, G.; Marca, S. Evaluation and Forecasting of Elapsed Fatigue Life of Ship Structures by Analyzing Data from Full Scale Ship Structural Monitoring. *J. Shipp. Ocean. Eng.* **2015**, *5*, 59–74.
42. Svendsen, B.T.; Tygesen, U.T.; Rosenville, J.K.; Azam, N. The use of digital solutions and structural health monitoring for integrity management of offshore structures. *Energy* **2022**, *2022*, 1100046947.
43. Stull, C.J.; Earls, C.J.; Koutsourelakis, P.S. Model-based structural health monitoring of naval ship hulls. *Comput. Methods Appl. Mech. Eng.* **2011**, *200*, 1137–1149. [[CrossRef](#)]
44. Yang, Y.C.; Chadha, M.; Hu, Z.; Vega, M.A.; Parno, M.D.; Todd, M.D. A probabilistic optimal sensor design approach for structural health monitoring using risk-weighted f-divergence. *Mech. Syst. Signal Process.* **2021**, *161*, 107920. [[CrossRef](#)]
45. Wolpert, D.H. The supervised learning no-free-lunch theorems. *Soft Comput. Ind.* **2002**, *2002*, 25–42.